# Aerodynamic Loads on Tall Buildings: Interactive Database

Yin Zhou. M.ASCE[1]; Tracy Kijewski, S.M.ASCE[2]; and Ahsan Kareem, M.ASCE[3]

**Abstract:** Under the action of wind, tall buildings oscillate simultaneously in the alongwind, acrosswind, and torsional directions. While the alongwind loads have been successfully treated using quasi-steady and strip theories in terms of gust loading factors, the acrosswind and torsional loads cannot be treated in this manner, since these loads cannot be related in a straightforward manner to the fluctuations in the approach flow. Accordingly, most current codes and standards provide little guidance for the acrosswind and torsional response. To fill this gap, a preliminary, interactive database of aerodynamic loads is presented, which can be accessed by any user with Microsoft Explorer at the URL address http://www.nd.edu/~nathaz/. The database is comprised of high-frequency base balance measurements on a host of isolated tall building models. Combined with the analysis procedure provided, the nondimensional aerodynamic loads can be used to compute the wind-induced response of tall buildings. The influence of key parameters, such as the side ratio, aspect ratio, and turbulence characteristics for rectangular sections, is also discussed. The database and analysis procedure are viable candidates for possible inclusion as a design guide in the next generation of codes and standards.

**DOI:** 10.1061/(ASCE)0733-9445(2003)129:3(394)

**CE Database keywords:** Aerodynamics; Wind loads; Wind tunnels; Databases; Random vibration; Buildings, high-rise; Turbulence.

## Introduction

Under the action of wind, typical tall buildings oscillate simultaneously in the alongwind, acrosswind, and torsional directions. It has been recognized that for many high-rise buildings the acrosswind and torsional response may exceed the alongwind response in terms of both serviceability and survivability designs (e.g., Kareem 1985). Nevertheless, most existing codes and standards provide only procedures for the alongwind response and provide little guidance for the critical acrosswind and torsional responses. This is partially attributed to the fact that the acrosswind and torsional responses, unlike the alongwind, result mainly from the aerodynamic pressure fluctuations in the separated shear layers and wake flow fields, which have prevented, to date, any acceptable direct analytical relation to the oncoming wind velocity fluctuations. Further, higher-order relationships may exist that are beyond the scope of the current discussion (Gurley et al. 2001).

Wind tunnel measurements have thus served as an effective alternative for determining acrosswind and torsional loads. For example, the high-frequency base balance (HFBB) and aeroelastic model tests are presently used as routine tools in commercial design practice. However, considering the cost and lead time needed for wind tunnel testing, a simplified procedure would be desirable in the preliminary design stages, allowing early assessment of the structural resistance, evaluation of architectural or structural changes, or assessment of the need for detailed wind tunnel tests. Two kinds of wind tunnel-based procedures have been introduced in some of the existing codes and standards to treat the acrosswind and torsional response. The first is an empirical expression for the wind-induced acceleration, such as that found in the National Building Code of Canada (NBCC) (NRCC 1996), while the second is an aerodynamic-load-based procedure such as those in Australian Standard (AS 1989) and the Architectural Institute of Japan (AIJ) Recommendations (AIJ 1996). The latter approach offers more flexibility as the aerodynamic load provided can be used to determine the response of any structure having generally the same architectural features and turbulence environment of the tested model, regardless of its structural characteristics. Such flexibility is made possible through the use of well-established wind-induced response analysis procedures. Meanwhile, there are some databases involving isolated, generic building shapes available in the literature (e.g., Kareem 1988; Choi and Kanda 1993; Marukawa et al. 1992), which can be expanded using HFBB tests. For example, a number of commercial wind tunnel facilities have accumulated data of actual buildings in their natural surroundings, which may be used to supplement the overall loading database. Though such HFBB data has been collected, it has not been assimilated and made accessible to the worldwide community, to fully realize its potential. Fortunately, the Internet now provides the opportunity to pool and archive the international stores of wind tunnel data.

This paper takes the first step in that direction by introducing an interactive database of aerodynamic loads obtained from HFBB measurements on a host of isolated tall building models, accessible to the worldwide Internet community via Microsoft Explorer at the URL address http://www.nd.edu/~nathaz. Through the use of this interactive portal, users can select the

[1]Engineer, Malouf Engineering International, Inc., 275 W. Campbell Rd., Suite 611, Richardson, TX 75080; Fomerly, Research Associate, NatHaz Modeling Laboratory, Dept. of Civil Engineering and Geological Sciences, Univ. of Notre Dame, Notre Dame, IN 46556. E-mail: yzhou@nd.edu

[2]Graduate Student, NatHaz Modeling Laboratory, Dept. of Civil Engineering and Geological Sciences, Univ. of Notre Dame, Notre Dame, IN 46556. E-mail: tkijewsk@nd.edu

[3]Robert M. Moran Professor, Dept. of Civil Engineering and Geological Sciences, Univ. of Notre Dame, Notre Dame, IN 46556. E-mail: kareem@nd.edu.

Note. Associate Editor: Bogusz Bienkiewicz. Discussion open until August 1, 2003. Separate discussions must be submitted for individual papers. To extend the closing date by one month, a written request must be filed with the ASCE Managing Editor. The manuscript for this paper was submitted for review and possible publication on April 24, 2001; approved on December 11, 2001. This paper is part of the ***Journal of Structural Engineering***, Vol. 129, No. 3, March 1, 2003. ©ASCE, ISSN 0733-9445/2003/3-394–404/$18.00.

geometry and dimensions of a model building, from the available choices, and specify an urban or suburban condition. Upon doing so, the aerodynamic load spectra for the alongwind, acrosswind, or torsional response is displayed along with a Java interface that permits users to specify a reduced frequency of interest and automatically obtain the corresponding spectral value. When coupled with the concise analysis procedure, discussion, and example provided, the database provides a comprehensive tool for computation of the wind-induced response of tall buildings.

## Wind-Induced Response Analysis Procedure

Using the aerodynamic base bending moment or base torque as the input, the wind-induced response of a building can be computed using random vibration analysis by assuming idealized structural mode shapes, e.g., linear, and considering the special relationship between the aerodynamic moments and the generalized wind loads (e.g., Tschanz and Davenport 1983; Zhou et al. 2002). This conventional approach yields only approximate estimates of the mode-generalized torsional moments and potential inaccuracies in the lateral loads if the sway mode shapes of the structure deviate significantly from the linear assumption. As a result, this procedure often requires the additional step of mode shape corrections to adjust the measured spectrum weighted by a linear mode shape to the true mode shape (Vickery et al. 1985; Boggs and Peterka 1989; Zhou et al. 2002). However, instead of utilizing conventional generalized wind loads, a base-bending-moment-based procedure is suggested here for evaluating equivalent static wind loads and response. As discussed in Zhou et al. (2002), the influence of nonideal mode shapes is rather negligible for base bending moments, as opposed to other quantities like base shear or generalized wind loads. As a result, base bending moments can be used directly, presenting a computationally efficient scheme, averting the need for mode shape correction and directly accommodating nonideal mode shapes. Application of this procedure for the alongwind response has proven effective in recasting the traditional gust loading factor approach in a new format (Zhou et al. 1999; Zhou and Kareem 2001). The procedure can be conveniently adapted to the acrosswind and torsional response (Boggs and Peterka 1989; Kareem and Zhou 2003). It should be noted that the response estimation based on the aerodynamic database is not advocated for acrosswind response calculations in situations where the reduced frequency is equal to or slightly less than the Strouhal number (Simiu and Scanlan 1996; Kijewski et al. 2001). In such cases, the possibility of negative aerodynamic damping, a manifestation of motion-induced effects, may cause the computed results to be inaccurate (Kareem 1982).

Assuming a stationary Gaussian process, the expected maximum base bending moment response in the alongwind or acrosswind directions or the base torque response can be expressed in the following form:

$$\hat{\boldsymbol{M}} = \overline{M} + g \times \sigma_{\boldsymbol{M}} \tag{1}$$

where $\hat{\boldsymbol{M}}$ and $\overline{M}$ = expected extreme value and mean of the moment or torque response, respectively; $g$ = peak factor; and $\sigma_{\boldsymbol{M}}$ = root mean square (RMS) of the fluctuating base moment or base torque response, which can be computed by $\sigma_{\boldsymbol{M}} = (\int_0^\infty S_{\boldsymbol{M}}(f)\,df)^{1/2}$ where $S_{\boldsymbol{M}}(f)$ = power spectral density (PSD) of the fluctuating base moment or torque response. It can be shown that the PSD of the moment response can be computed by the following equation (Zhou and Kareem 2001):

$$S_{\boldsymbol{M}}(f) = S_M(f)|H_1(f)|^2 \tag{2}$$

where $|H_1(f)|^2 = \{[1-(f/f_1)^2]^2 + (2\zeta_1(f/f_1))^2\}^{-1}$ = structural first mode transfer function; $f_1$ and $\zeta_1$ = natural frequency and critical damping ratio in the first mode, respectively; and $S_M(f)$ = PSD of the external aerodynamic base moment or torque. The flexibility to consider nonideal mode shapes and nonuniform mass distributions has been addressed in Eq. (2) (Boggs and Peterka 1989; Zhou et al. 1999, 2002). Note that the same symbol, but expressed in bold, is employed here to distinguish the base moment or base torque response from the external aerodynamic moment or torque. The former includes the dynamic amplification effects due to wind fluctuations and structural dynamics.

To facilitate computations, the integration in Eq. (2) is divided into two portions, i.e., background and resonant components. The resonant base moment or base torque response, $\hat{\boldsymbol{M}}_R$ can be computed in closed form by assuming that the excitation can be represented by white noise in the vicinity of the structure's natural frequency and by subsequently invoking the Residue Theorem for integration

$$\hat{\boldsymbol{M}}_R = g_R \sqrt{\frac{\pi}{4\zeta_1} f_1 S_M(f_1)} \tag{3}$$

where $g_R = \sqrt{2\ln(f_1 T)} + 0.5772/\sqrt{2\ln(f_1 T)}$ = resonant peak factor; $T$ = observation time; and subscript $R$ = resonant component. The background base moment and base torque $\hat{\boldsymbol{M}}_B$ is equal to the aerodynamic quantity, since for the background response the structure responds statically with a dynamic magnification factor of unity, and

$$\hat{\boldsymbol{M}}_B = g_B \times \sigma_M \tag{4}$$

where $g_B$ = background peak factor, which is usually at 3–4; $\sigma_M$ = RMS aerodynamic moment; and subscript $B$ = background component.

The mean base moment or base torque can be estimated from the HFBB test or by a mean pressure measurement test that is usually used as a companion test for the design of the cladding system.

With the known base moment and base torque response, the equivalent static wind loading can be obtained by distributing the base moment to each floor in an appropriate manner as detailed in Zhou and Kareem (2001) and Kareem and Zhou (2003). The equivalent static wind loads at height $z$ for sway motions, can be computed by

$$\hat{\boldsymbol{P}}_R(z) = \hat{\boldsymbol{M}}_R \frac{m(z)\varphi_1(z)}{\int_0^H m(z)\varphi_1(z)\cdot z\,dz} \tag{5}$$

while for the torsional case

$$\hat{\boldsymbol{P}}_R(z) = \hat{\boldsymbol{M}}_R \frac{I(z)\varphi_1(z)}{\int_0^H I(z)\varphi_1(z)\,dz} \tag{6}$$

where $\hat{\boldsymbol{P}}_R$ = resonant component of the equivalent static wind loading; $m(z)$ = mass per unit height; $I(z)$ = mass moment of inertia per unit height; and $\varphi_1(z)$ = fundamental mode shape in the direction of motion.

The wind-induced response, including the overall deflection, acceleration, internal forces, and stresses in each structural member can be computed using the equivalent static wind loads with a simple static analysis. For any response component, the resultant effect can be determined by summing the mean and the square root of the sum of the squares (SRSS) combination of the background and resonant components

**Table 1.** Model Sections

| Model | 1 | 2 | 3 | 4 | 5 | 6 | 7 | 8 | 9 |
|---|---|---|---|---|---|---|---|---|---|
| D:B | 2:6 | 3:6 | 4:6 | 4:4 | 6:4 | 6:3 | 6:2 | 4:4 | 4:6(60°) |
| Shape |  | | | | | | | | |
| |  | | | | | | | | |

Oncoming wind

$$\hat{r}=\overline{r}+\sqrt{\hat{r}_B^2+\hat{r}_R^2} \tag{7}$$

where $\hat{r}$ = resultant wind-induced response of interest and $\overline{r}$, $\hat{r}_B$, $\hat{r}_R$ = mean, peak background, and peak resonant response components, respectively, which are computed using the corresponding equivalent static wind load component with static analysis.

However, for the acceleration response, only the resonant component is of interest. For example, the peak acceleration in the sway mode can be computed by

$$\hat{\ddot{Y}}(z)=\frac{\int_0^H \hat{\mathbf{P}}_R(z)\varphi_1(z)dz}{\int_0^H m(z)\varphi_1^2(z)dz}\varphi_1(z) \tag{8}$$

In the case of the torsional response, the mass per unit height, $m(z)$, in Eq. (8) is replaced by $I(z)$, the mass moment of inertia per unit height. The resulting RMS acceleration can then be determined by dividing the peak accelerations by the resonant peak factor $g_R$.

## Experimental Procedure

### Building Models

As shown in Table 1, nine building cross sections were tested on an ultra-sensitive force balance. Three different rigid balsa wood models of each cross section were constructed, with heights of 16, 20, and 24 in. yielding 27 different model buildings of varying aspect ratio and shape to investigate the influence of structural dimensions on aerodynamic loads. Photographs of the actual lightweight, building models are provided in Kijewski and Kareem (1998).

### Wind Tunnel Testing Conditions

Each of the balsa wood models was tested in a boundary layer wind tunnel with a 10 ft×5 ft cross section and 60 ft length (Kareem 1990). The turbulent boundary layers simulated in this study were generated by the natural action of surface roughness added on the tunnel floor and by upstream spires. Two approach flows, namely, BL1 ($\alpha=0.16$, where $\alpha$ = exponent of mean wind velocity profile) and BL2 ($\alpha=0.35$), corresponding, respectively, to an open and an urban wind environment, were simulated. The boundary layer thickness in BL1 and BL2 was 40 and 47 in., respectively, while the longitudinal length scale between the heights of 10 and 30 in. varied from 12 to 20 in., and turbulent fluctuations conformed to the prescribed spectral description (Kareem and Cheng 1984). The simulated boundary layer profiles are shown in Fig. 1. A constant-temperature hot-film anemometer was used to map the flow field characteristics in the tunnel. A detailed description of the test and validation of the accuracy of the force balance technique can also be found in Kijewski and Kareem (1998). In order to evaluate the influence of aspect ratio and side ratio within the data set, only the rectangular plan data are discussed herein.

### Data Processing

The output of the sensitive, multicomponent force balance was recorded over a 5-min interval at sampling rate of 300 Hz. The resulting time histories were segmented into blocks, analyzed by a 4,096-point fast Fourier transform, to yield over 20 raw spectra, which were subsequently ensemble averaged. Prior to each test, system identification was conducted on the base balance mounted with each balsa wood model to ascertain the system transfer function. This information was then used to digitally correct the data for potential dynamic amplitude or phase distortion.

### Data Preparation

In this discussion and the accompanying online database, the measured aerodynamic loads are defined in terms of the RMS base moment coefficient and the nondimensional PSD as follows:

$$\sigma_{C_M}=\sigma_M/\overline{M}' \tag{9}$$

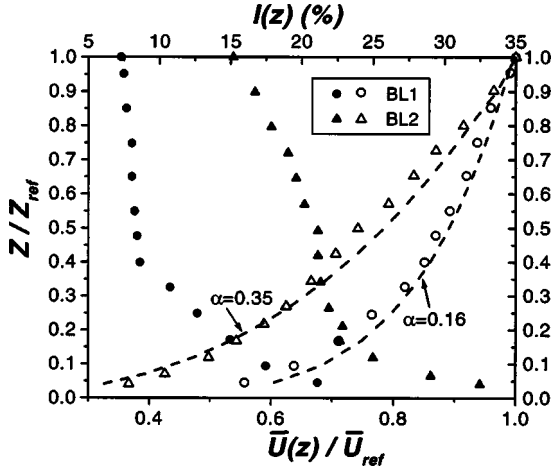


**Fig. 1.** Modeling boundary layers

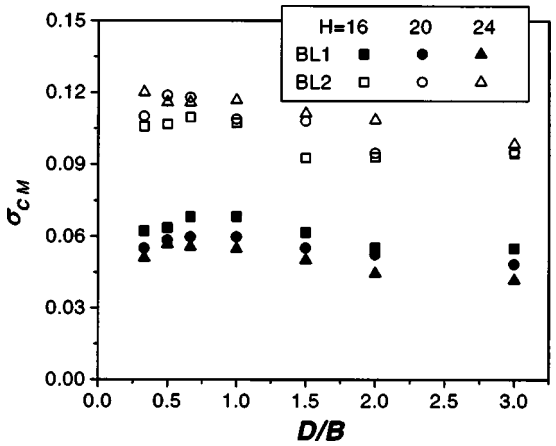


**Fig. 2.** RMS coefficients of alongwind aerodynamic base moments

$$C_M(f)=(f\times S_M(f))/\sigma_M^2 \tag{10}$$

where $C_M$ = nondimensional moment coefficient and $\overline{M}'$ = reference moment or torque, which is defined by $\overline{M}'_D=(1/2\rho\overline{U}_H^2BH^2)$, $\overline{M}'_L=(1/2\rho\overline{U}_H^2DH^2)$, and $\overline{M}'_T=(1/2\rho\overline{U}_H^2BDH)$ for the alongwind, acrosswind, and torsional directions, respectively. Here, $\rho$ = air density; $B$ = building width normal to the oncoming wind; $D$ = building depth; $\overline{U}_H$ = mean wind velocity evaluated at the building height $H$; and subscripts $D$, $L$, and $T$ = alongwind, acrosswind, and torsional directions, respectively. It is noteworthy that, except for the alongwind load, different definitions have been used in the literature, e.g., $D$ is replaced with a $B$ for the acrosswind load, and $BD$ is expressed in terms of $B^2$ for the torque (Marukawa et al. 1992; Choi and Kanda 1992; Kijewski and Kareem 1998). These definitions will lead to marked differences in the RMS coefficients in Eq. (9), while having no impact on the normalized spectrum in Eq. (10).

The nondimensional aerodynamic loads can be directly used in the above wind-induced response analysis procedure, e.g., the background and resonant components of the base bending moment or base torque response can be computed, respectively, by

$$\hat{\boldsymbol{M}}_B=g_B\times\sigma_{C_M}\times\overline{M}' \tag{11}$$

$$\hat{\boldsymbol{M}}_R=g_R\times\sigma_{C_M}\times\overline{M}'\sqrt{\frac{\pi}{4\zeta_1}C_M(f_1)} \tag{12}$$

It can be seen from Eqs. (11) and (12) that the RMS coefficient is important for both the background and the resonant components. For the resonant response, the spectral value around the structural natural frequency in the first mode is of most significance. When making a comparison between the background and the resonant response components, the latter could be larger depending on whether or not the radical term in Eq. (12) is larger than unity. Since the damping of the structure used in wind resistant analysis is usually very small, e.g., 1%, this term is larger than one when the normalized spectral coefficient is above 0.013. Furthermore, a 10% error in the RMS coefficient will lead to 10% error in estimates of both the background and the resonant response. However, the error in the spectral value impacts only the RMS resonant response in proportion to its half power. It is important to note that this quantity is quite sensitive to the modeling of the approach flow characteristics. In Simiu and Scanlan (1996), a summary of acrosswind force coefficients for simple geometric shapes measured in different wind tunnel facilities are compared. The data exhibit wide scatter.

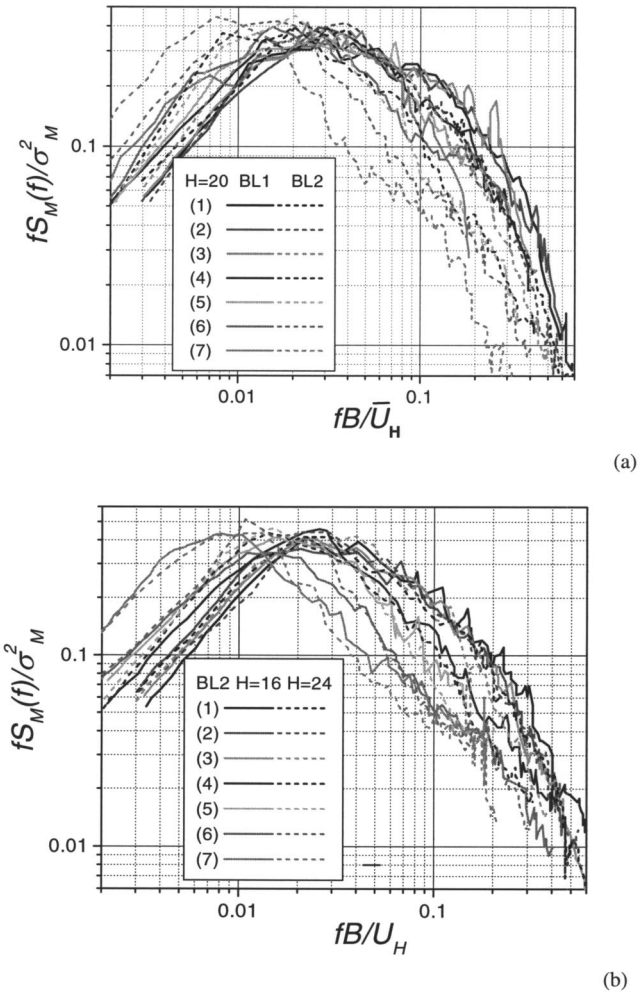


**Fig. 3.** Spectra of alongwind aerodynamic base moments (a) influence of turbulence intensity and (b) influence of aspect ratio

In light of this discussion, it becomes evident that precise estimates of the RMS and spectral value are critical to providing accurate aerodynamic load information. Though the empirical fits to experimental data provide compact representations for use in some codes and standards, they cannot accurately fit the experimental data over all frequencies. On the other hand, the direct use of experimental data provides precise estimates of spectral values along with the flexibility to consider a variety of geometries, dimensions and turbulence conditions.

## Aerodynamic Loads

In this paper, only the aerodynamic loads with a zero angle of attack on the rectangular models are discussed. It is noteworthy that Models 1, 2, and 3 correspond to Models 7, 6, and 5 with a 90° change of attack angle, respectively. Note that while Figs. 3, 5, 7 and 8 appear in grayscale, those desiring to study these figures in more detail may wish to view the color versions available through the PDF file at www.nd.edu/~nathaz/database/paper.pdf.

### *Alongwind*

#### RMS Coefficient

The alongwind RMS moment coefficient manifests dependence on the side ratio D/B (Fig. 2). When D/B$\leqslant$1.0, the coefficient is

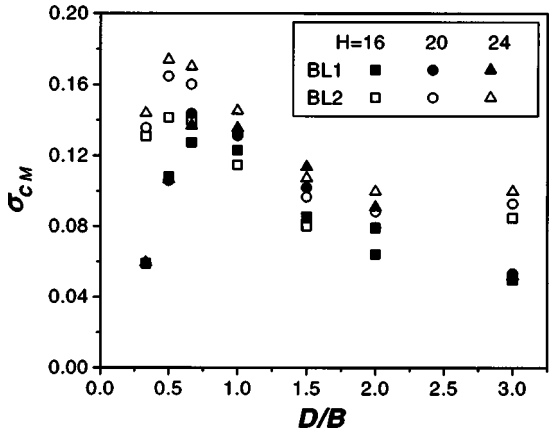


**Fig. 4.** RMS coefficients of acrosswind aerodynamic base moments

nearly constant, while the coefficient decreases as the side ratio increases from unity. This trend is consistent with that of the mean drag coefficient in the Australian Standard (AS 1989). The turbulence field significantly affects the RMS coefficient, which increases approximately in proportion to the turbulence intensity as the approach flow changes from BL1 to BL2, while there is only moderate sensitivity to the aspect ratio. In BL1, the larger the aspect ratio, the less the RMS force coefficient; however, in BL2, this trend is reversed.

**Spectrum**

The discussion of the wind load spectra will be limited to the high-reduced frequency range, i.e., $f^*=fB/\overline{U}_H>0.1$, which encompasses the wind velocity range of operation of most tall buildings. The alongwind spectra are very close to each other in the range when D/B$<$1.0, while decreasing as the side ratio increases from unity (Fig. 3). With the increase in the side ratio, the afterbody length increases, which results in the reattachment of flow that vitiates the organized wake fluctuations. The increase in the turbulence intensity generally reduces the spectra at higher frequencies as shown in Fig. 3(a). The increase in turbulence also promotes earlier reattachment, similar to the increase in afterbody length, which results in reducing wake fluctuations in the high-frequency range. The spectrum is relatively insensitive to the aspect ratio as shown in Fig. 3(b).

### *Acrosswind*

**RMS Coefficient**

The acrosswind RMS moment coefficient depends markedly on the side ratio, as shown in Fig. 4. It increases with the side ratio for D/B$<$0.67, while decreasing as D/B increases from 0.67. When D/B$\leqslant$0.67 and D/B$=$3.0, the higher the turbulence, the larger the moment coefficient, while side ratios between 0.67 and 2 have RMS coefficients that are not sensitive to the turbulence. The moment coefficient is relatively insensitive to the aspect ratio, although generally, the higher the aspect ratio, the larger the moment coefficient.

**Spectrum**

Unlike the alongwind spectrum, the acrosswind spectrum exhibits an evident peak around the Strouhal number as shown in Fig. 5. The amplitude and bandwidth of the spectrum depend mainly on the side ratio, although generally, the higher the peak value, the

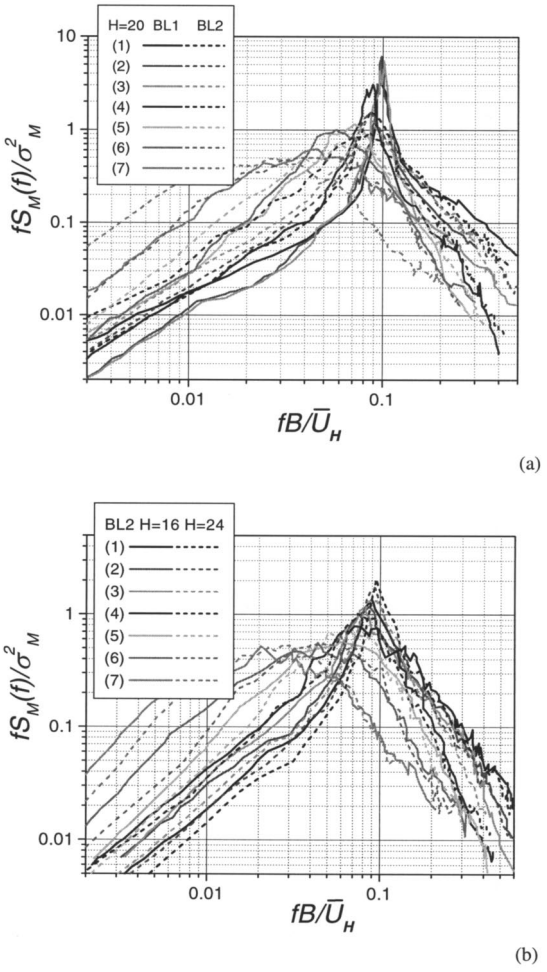


**Fig. 5.** Spectra of acrosswind aerodynamic base moments (a) influence of turbulence intensity and (b) influence of aspect ratio

narrower the spectrum. The frequency where the peaks occur depends on the definition of the reduced frequency $f^*$, which is consistently defined as $fB/\overline{U}_H$ for all three directions in this discussion. When using this definition, the reduced frequencies corresponding to the peaks are 0.1 when D/B$<$1.0, 0.09 when D/B $=$1.0, and rapidly decrease as D/B increases from 1.0 for the case

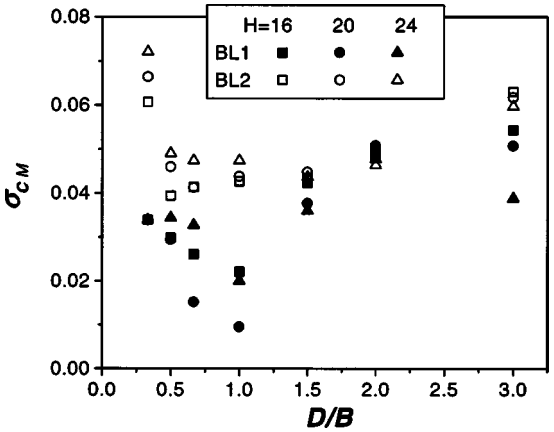


**Fig. 6.** RMS coefficients of aerodynamic base torques

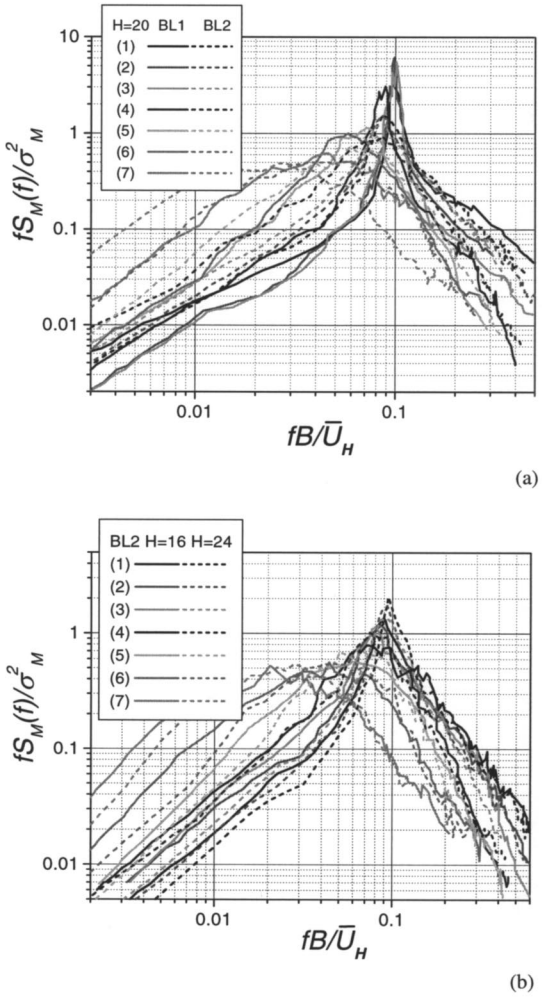


**Fig. 7.** Spectra of aerodynamic base torques (a) influence of turbulence intensity and (b) influence of aspect ratio

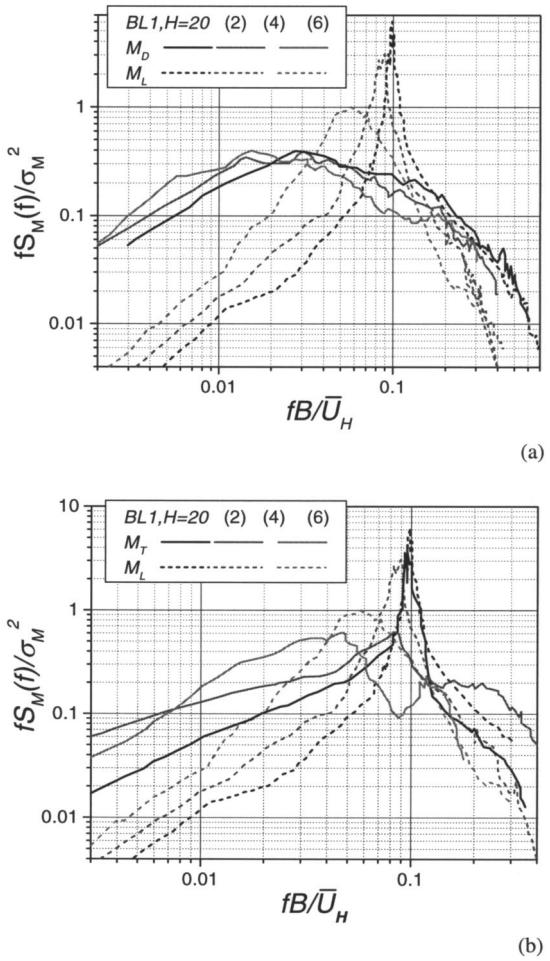


**Fig. 8.** Comparison between aerodynamic components (BL1, $H=20$) (a) alongwind and acrosswind and (b) acrosswind and torsional

of BL1 and $H=20$. The spectral value in the high-frequency range decreases rapidly with frequency. While lower-side ratios produce larger spectral values, an increase in turbulence generally lowers the peak, broadens the spectral bandwidth, and shifts the peak to a slightly lower-reduced frequency as shown in Fig. 5(a). Similar effects of turbulence have been noted by Kareem and Cermak (1984) in examining the space-time variations of pressure fluctuating on a square cross-section building model. The spectral values in the high-frequency range are relatively insensitive to turbulence, though Model 7 does display a more obvious departure. In Fig. 5(b), the larger aspect ratio may marginally increase the peak value, shifting the peak towards a slightly higher frequency and narrowing the spectral bandwidth. The magnitude of the spectrum in the high-frequency range is very insensitive to the aspect ratio. Further details regarding the structure of random pressure fields on prismatic bodies can be found in Kareem (1997) and Haan et al. (1998).

## *Torsion*

### RMS Coefficient

The torsional RMS coefficient is very sensitive to the side ratio as shown in Fig. 6. The coefficient decreases with increasing side ratio D/B up to 1.0, while increasing with D/B beyond this point. Increased turbulence yields markedly larger base torque coefficients only when $D/B<1.0$, while the sensitivity to aspect ratio is only moderate and substantially diminished for $1.5\leqslant D/B\leqslant 2.0$.

### Spectrum

The base torque spectrum is considerably sensitive to the side ratio as illustrated in Fig. 7(a). In BL1, when $D/B\leqslant 0.5$, the spectrum has one peak at the same reduced spectrum as the acrosswind base moment spectrum. When $D/B>0.5$, the spectrum has two peaks, the first, a more narrowband peak at a reduced frequency close to that of the acrosswind spectrum and the second at a higher-reduced frequency, with reduced magnitude and larger bandwidth. The first peak results from the unsymmetrical nature of vortex shedding, whereas the second peak arises from the reattachment and subsequent reseparation of the flow due to the increase in afterbody length or flapping of the shear layers. Note that more detailed scenarios of flow patterns around buildings are possible for specific cross sections. Both the first and the second peaks shift towards lower-reduced frequencies as the side ratio increases. Since the reduced frequency for the torsional response analysis is usually higher than that of the alongwind and acrosswind directions, the spectrum value around the second peak may have significant contributions to the torsional response.

The increase in turbulence clearly affects the peaks, i.e., it lowers the first peak value and slightly shifts the peaks to a lower-

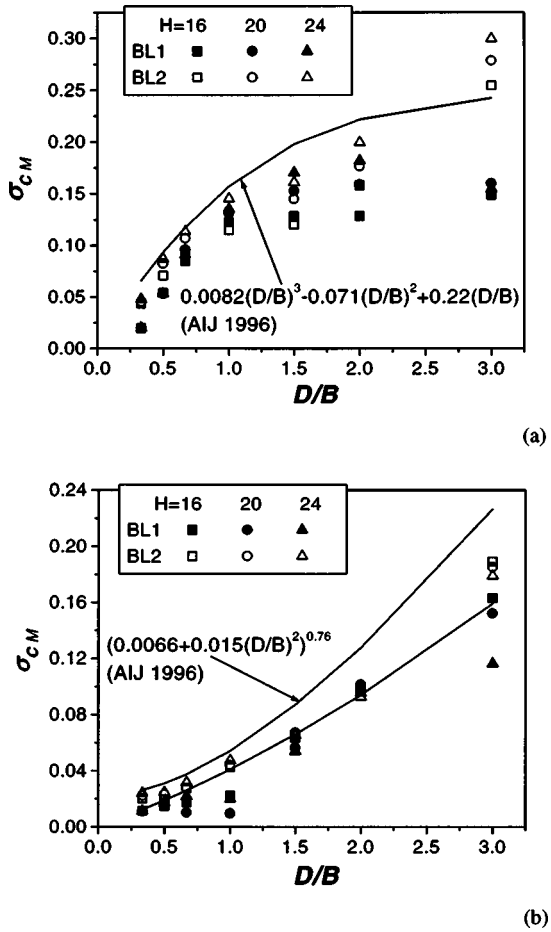


**Fig. 9.** Comparison of RMS coefficients with AIJ (1996) data (a) acrosswind in $\sigma_M/(1/2\rho\bar{U}_H^2BH^2)$ and (b) torsion in $\sigma_M/(1/2\rho\bar{U}_H^2B^2H)$

reduced frequency, while it completely suppresses the second peak for all side ratios. The disappearance of the second peak stems from the fact that the reattachment due to the increased turbulence reduces the energy of the fluctuating pressure, which concomitantly influences the resulting torque.

The torque spectrum is relatively sensitive to the aspect ratio. The increase of the aspect ratio in Fig. 7(b) leads to the magnification of the first peak value, while significantly restraining the second peak, thereby reducing the value of the torque spectrum at higher reduced frequencies.

### Comparison Between Aerodynamic Load Components

A comparison of the aerodynamic load spectra of representative cross sections is presented here. First, the alongwind and acrosswind spectra are compared, and then the acrosswind and torsional cases are considered to discern any common features that may shed light on their genesis. For the cases shown in Fig. 8(a), the acrosswind moment spectrum is more narrow-banded in character and takes on much larger values in the vicinity of its peak, in comparison with the alongwind direction. The difference in the spectral features clearly confirms the different mechanisms of excitation in the two directions of loading. In Fig. 8(b), the alignment of the first peak in the torque and the acrosswind spectra reaffirms the contribution of antisymmetric loading patterns induced by vortex shedding to both of these components. Meanwhile, the existence of a second peak in the torque spectrum alone

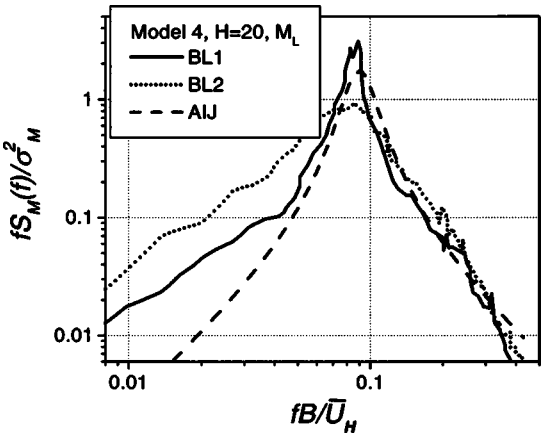


**Fig. 10.** Comparison of acrosswind spectra with AIJ (1996) data

reflects a suite of other possible mechanisms, of which the most plausible one arises from the secondary reattachment and reseparation of shear layers on cross sections with longer afterbodies or flapping of the shear layers.

### Comparison with Available Data

The data in this paper are also compared with those in the available literature. Figs. 9(a and b) shows the results of the comparison of the RMS base moment coefficients for the acrosswind and torsional directions based on the data provided in this study with the AIJ standard (AIJ 1996). Note that the AIJ expression is solely a function of the side ratio, since the dispersion in their data has not confirmed dependence on turbulence intensity. With one exception, the AIJ expression conservatively predicts the RMS moment coefficient. Note that this exception is also the instance for which the experimental data manifests the most marked dependence on turbulence intensity and height (corresponding to D/B $=3.0$). Once again, as marked dependence on terrain was not observed in the AIJ data, the expression developed by the AIJ standard for the acrosswind moment spectra also does not implicitly consider the influence of turbulence, but instead provides a spectrum that effectively represents a suburban terrain. It should not be surprising then to see that AIJ's acrosswind spectrum for a square building compares well with the suburban spectra (BL1) provided by this study (Fig. 10). Considering the difference in the test conditions, the relatively good agreement suggests, on the one hand, the effectiveness of the data in this paper, on the other hand, the applicability of the aerodynamic-load-based procedure for the preliminary design. This good comparison of data is also a reflection of the improvement in HFBB techniques, quality of the resulting measurements, and an improved and consistent simulation of the approach flow, as compared to an earlier comparison where most of the data for similar building shapes exhibited appreciable variations (Simiu and Scanlan 1996).

## Access to the Database

The compact empirical formula supplied by the AIJ standard (AIJ 1996), in general, provides acceptable agreement with the experimental data. However, as the expression was developed as a best fit to a number of side/aspect ratios, there can be considerable deviation from the actual experimental data for specific side ratios or frequency ranges. Such deviations, as discussed previously, can

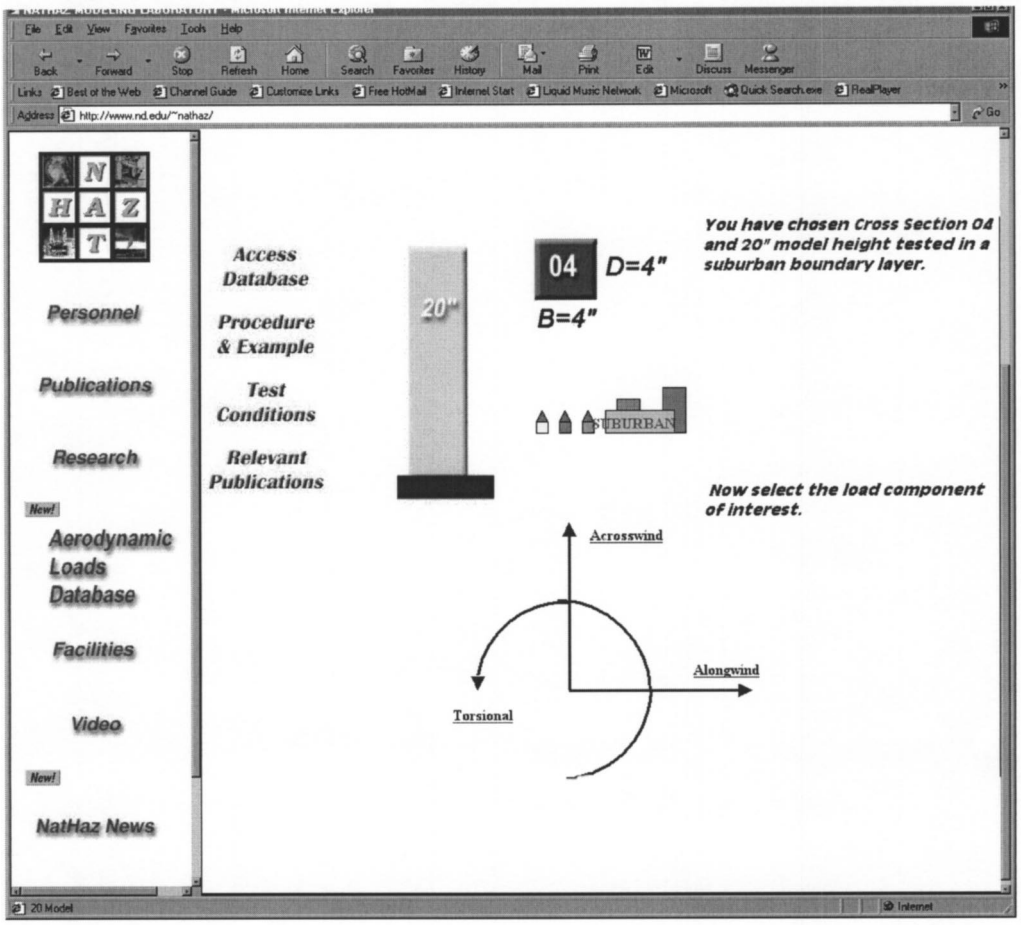


**Fig. 11.** Aerodynamic Loads Database gateway for selection of desired aerodynamic load spectra

have notable impacts on the predicted response. Direct use of the spectral data can bypass the opportunity for the errors introduced by curve-fit expressions, which are currently constrained to only rectangular shapes, being a function of the building's side and aspect ratios, limiting the structures that can be considered. Fortunately, the Internet provides an internationally accessible platform for archiving experimental results, permitting the efficient presentation of actual data for a host of geometries, dimensions, and turbulence conditions. For the purpose of codification, the spectrum for a given geometry, dimension, and turbulence condition can be presented digitally on line. This digital spectrum, in order to alleviate the bias errors associated with individual experiments, can be an average of several independent wind tunnel tests, each conducted with sufficient data to reduce statistical errors. In this manner, the reliability of the spectrum can be insured without over generalizing the spectrum using a curve fit expression designed to satisfy a host of aspect ratios.

The first step towards such a database has been initiated at http://www.nd.edu/~nathaz through the *Aerodynamic Loads Database* available to Microsoft Explorer users. Upon entrance to the database, the user will step through a series of links to identify, with certainty, the data of interest. Once the desired building model has been selected, the database will recap the selections and prompt the user to select the alongwind, acrosswind, or torsional load results, as shown in Fig. 11.

*JAVA* programming was used to create an interface that allows the retrieval of a specific value of the non-dimensional power spectrum. The interface, shown in Fig. 12, displays the entire nondimensional power spectrum and then allows the user to input an arbitrary value of the nondimensional frequency in order to obtain the corresponding spectral value, as would be done to determine the value of the power spectrum at the fundamental frequency of the structure. The use of digitized spectra removes the opportunity for human errors that result from picking off values from hard-copy spectra and eliminate the uncertainty associated with curve-fit expressions. In addition, the calculated RMS coefficient is also provided.

After obtaining the value of the nondimensional power spectrum and associated RMS coefficient, the user can access a detailed summary of the procedure necessary to calculate the corresponding global response, with an example provided for clarity. Additional database resources include a description of the test conditions and relevant publications.

Through the cooperative efforts of a host of research groups, codes, and standards need no longer limit themselves to approximate expressions for rectangular shapes of limited side ratio, as the data contained herein can be expanded to include a variety of shapes, aspect ratios, side ratios, and wind conditions to provide reliable load spectra for a wide range of structures. The *Aerodynamic Loads Database* at the NatHaz Modeling Laboratory provides a prototype to launch the concept of the next generation of codes and standards for high-rise buildings with the promise of expansion to more sophisticated databases.

## Example

While the example provided online (www.nd.edu/~nathaz/database/procedure.html) is more detailed, an abbreviated version

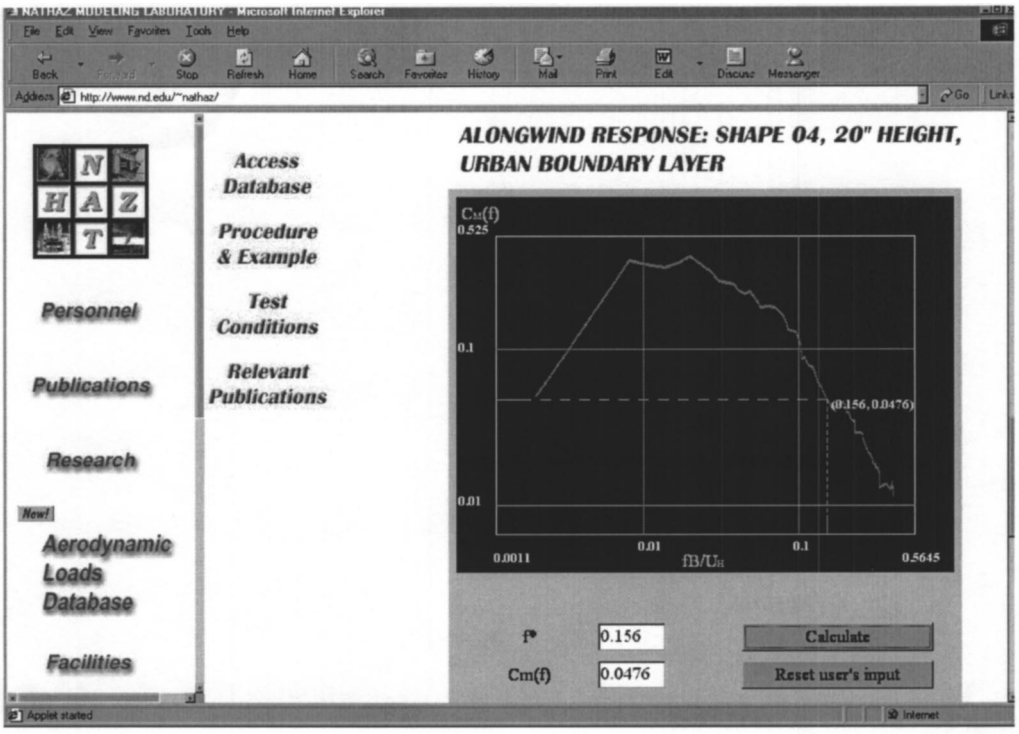


**Fig. 12.** Aerodynamic Loads Database interface: User input nondimensional frequency and nondimensional power spectral value provided by *JAVA* script

is provided here to illustrate the general application of the wind-induced response analysis procedure discussed in this paper. For simplicity, the influences of wind direction, topography, shielding, importance factor, and return period are ignored in the discussion herein. Table 2 summarizes the properties of the structure under consideration.

The first step in the procedure is to calculate the reduced frequency in terms of the mean wind speed at the building's full height in Exposure Category A. This requires several conversions: (1) convert the wind speed at 10 m height in from a 3-s gust in open terrain to a wind speed with averaging time of 1-h in Exposure A, and (2) bring that wind speed to the full height of the structure. This first series of calculations is outlined in Table 2(a). Two scenarios are considered, the survivability design with a 50-year event for determination of base moments, and the serviceability design with a 10-year event for determination of RMS acceleration levels.

The online database can then be used to retrieve the RMS moment coefficients and to determine the appropriate nondimensionalized spectral values for each reduced frequency calculated in Table 2(a). The specific case for this example would be the Shape 04, 20″ model tested in the urban terrain, which can be found by navigating the database or by going directly to www.nd.edu/~nathaz/database/shape04/ht20/urban/response.html. Table 2(b) lists the appropriate values, rounded to three decimal places for the purposes of this example. Note that Fig. 12 illustrates this use of the database for the alongwind survivability case, displaying the user input and corresponding *JAVA*-calculated output.

The evaluation of Eqs. (11) and (12) with the values provided by the database facilitates the computation of background and resonant components of the base bending moment and base torque, with the background peak factor $g_B$ assumed to be 3.4, in accordance with ASCE 7-98 (2000). While the mean base moment for the acrosswind and torsional response is assumed zero, the alongwind mean base moment can be calculated by integrating the mean loads over the height according to $\overline{M} = \int_0^H \overline{P}(z) z\, dz$, in which the mean wind load per unit height is given by $\overline{P}(z) = 1/2\rho \overline{U}_H^2 (z/H)^{2\alpha} B C_D$, where $C_D$ = drag force coefficient. The peak base moment can then be determined in accordance with the combination rule given by Eq. (7). The results for the survivability analysis are provided in Table 3(a), alongside estimates for the alongwind component obtained from ASCE 7-98 (2000). ASCE's peak base bending moment was obtained by similarly integrating the net pressures given by Eq. 6-17 in the ASCE standard over the building height. The mean base bending moment is then determined by dividing by the gust effect factor, calculated according to provisions in the standard. Note that while the code is conservative in its estimate, the results are still within about 7%.

In the case of serviceability design for human comfort considerations, RMS accelerations for a 10-year event become the critical consideration. Peak accelerations can be obtained by Eq. (8) and divided by the resonant peak factor to yield the RMS accelerations provided in Table 3(b). This requires the determination of the resonant component of the equivalent static wind loads, given by Eqs. (5) and (6), in addition to the resonant base moments. In the case of the torsional component, the mass moment of inertia per unit height in Eq. (6) is defined as $m(z)\gamma^2$, where $\gamma$ is the assumed radius of gyration. Note that the angular accelerations due to torsion may be separated into the resultant alongwind and acrosswind components at the corner of the structure, as shown by the figure inset in Table 3(b). These lateral accelerations induced by torsion can be combined with those generated by the sway motion to obtain the total lateral accelerations at the corner

**Table 2.** Example: Outline of Building and Approach Wind Characteristics and Intermediate Calculations

| | |
|---|---|
| Building dimensions: $B=40$ m, $D=40$ m, $H=200$ m, average radius of gyration $=18$ m | Damping ratio $\zeta=0.02$ (Composite Structural System) |
| Building natural frequency $f_{1x}=0.2$ Hz, $f_{1y}=0.2$ Hz, $f_{1z}=0.35$ Hz | Basic wind speed at reference height of 10 m in terms of 3-s gust, $U_{10}=63$ m/s (Fig. 6-1b, ASCE 7-98) |
| Building bulk density is 250 kg/m$^3$ | Air density $\rho=1.25$ kg/m$^3$ |
| Drag force coefficient $C_D=1.3$ | Linear mode shape in all directions |

Location: Urban zone along Atlantic Coast of South Florida. According to ASCE 7-98, this site is defined as Exposure A from all directions, with $\alpha=1/3.0$ (Table 6-4, ASCE 7-98)

(a) Step 1

Survivability design (one-hour averaging time, 50-year return period)

Wind speed at 10 m height in terms of 3-s gust in open terrain $=63$ m/s

(i) Conversion to wind speed in terms of 1-h mean in Exposure A $=63\times0.30^{a}=18.9$ m/s

(ii) Conversion to wind speed at 200 m height in terms of 1-h mean in Exposure A

$$\overline{U}_H=18.9\times(200/10)^{1/3}=51.30 \text{ m/s}$$

$f_{1x}B/\overline{U}_H=0.156$ $\quad$ $f_{1y}B/\overline{U}_H=0.156$ $\quad$ $f_{1z}B/\overline{U}_H=0.273$

Serviceability design (1-h averaging time, 10-year return period)

Conversion to 3-s gust at 10 m height in open terrain for 10-year return period $=63\times0.74^{b}=46.62$ m/s

(i) Conversion to 1-h mean wind speed in Exposure A $=46.62\times0.30^{a}=13.99$ m/s

(ii) Conversion to wind speed at 200 m height in terms of 1-h mean in Exposure A

$$\overline{U}_H=13.99\times(200/10)^{1/3}=37.96 \text{ m/s}$$

$f_{1x}B/\overline{U}_H=0.211$ $\quad$ $f_{1y}B/\overline{U}_H=0.211$ $\quad$ $f_{1z}B/\overline{U}_H=0.369$

(b) Step 2

| | $\sigma_{C_M}$ | $f_1B/\overline{U}_H$ | | $C_M(f_1)$ | |
|---|---|---|---|---|---|
| | | 50-year | 10-year | 50-year | 10-year |
| Alongwind | 0.109 | 0.156 | 0.211 | 0.048 | 0.040 |
| Acrosswind | 0.133 | 0.156 | 0.211 | 0.192 | 0.073 |
| Torsional | 0.044 | 0.273 | 0.369 | 0.059 | 0.040 |

[a]Conversion factor, $\overline{b}$, given from Table 6-4 (ASCE 7-98).

[b]Conversion factor given in Table C6-3 (ASCE 7-98).

**Table 3.** Example: Calculated Base Moments for Survivability Design and RMS Accelerations for Serviceability Design

(a) Base moments for survivability design ($10^6$ kN m)

| | $\bar{M}$ | $\hat{\mathbf{M}}_B$ | $\hat{\mathbf{M}}_R$ | $\hat{\mathbf{M}}$ |
|---|---|---|---|---|
| Alongwind by ASCE 7-98 | 3.28[a] | — | — | 3.31[b] |
| Alongwind | 1.28 | 0.97 | 1.49 | 3.06 |
| Acrosswind | 0.00 | 1.19 | 3.64 | 3.83 |
| Torsional | 0.00 | 0.08 | 0.14 | 0.16 |

(b) RMS accelerations at roof

| | |
|---|---|
| Alongwind by ASCE 7-98 | 3.84 m g |
| Alongwind | 3.76 m g |
| Acrosswind | 6.20 m g |
| Lateral accelerations at corner induced by torsion | $1.20\times10^{-3}$ rad/s$^2$ |
| | Alongwind component: 2.50 m g |
| | Acrosswind component: 2.50 m g |
| Total lateral accelerations at corner | Alongwind component: 4.52 m g |
| | Acrosswind component: 6.69 m g |

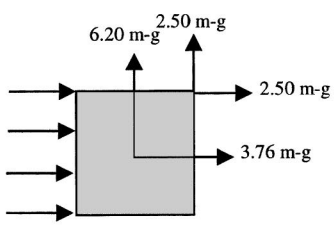


[a]Mean base moment, in 3-s averaging time. All other results in terms of 1-h averaging time. $\bar{M}=\hat{\mathbf{M}}/G$, where the gust effect factor, $G=1.01$ as determined by Eq. 6-6 (ASCE 7-98).

[b]Determined by net effect of pressures prescribed by Eq. 6-17 on windward and leeward faces, integrated over full height of structure.

by SRSS or complete quadratic combination. Once again, the ASCE 7-98 (2000) prediction for the alongwind RMS acceleration is provided for comparison and indicates that the code is only slightly conservative, with the two estimates being within a few percent.

## Concluding Remarks

This paper presents a preliminary Internet database of aerodynamic loads obtained from the HFBB measurements on a host of typical tall building models. The influence of key parameters, such as the side ratio, aspect ratio, and turbulence characteristics is discussed. The proposed database can be easily expanded utilizing HFBB tests. Analysis procedures, along with a detailed example, are also supplied to employ the aerodynamic load data in the computation of the wind-induced response of tall buildings with similar turbulence and geometrical features. The database and other relevant information are accessible to the community via Microsoft Explorer at the URL address http://www.nd.edu/~nathaz/. The database and the analysis procedure can be considered for possible inclusion in codes and standards as a design guide in the preliminary stages.

## Acknowledgments

The writers gratefully acknowledge the support provided in part by the National Science Foundation Grant Nos. BCS 90-96274, CMS 95-03779, CMS 95-22145, and CMS 00-85019, the NASA Indiana Space Grant, and the Center for Applied Mathematics at the University of Notre Dame.

## References

American Society of Civil Engineers (ASCE) (2000). *ASCE 7-98 minimum design loads for buildings and other structures*, Reston, Va.

Architectural Institute of Japan (AIJ) (1996). *Recommendations for loads-on buildings*, Tokyo.

Australian Standard (AS) (1989). *SAA Loading code, part 2—Wind forces, AS1170.2-89*, Sydney, Australia.

Boggs, D. W., and Peterka, J. A. (1989). ''Aerodynamic model tests of tall buildings.'' *J. Eng. Mech.*, 115(3), 618–635.

Choi, H., and Kanda, J. (1993). ''Proposed formulae for the power spectral densities of the fluctuating lift and torque on rectangular 3-D cylinders.'' *J. Wind. Eng. Ind. Aerodyn.*, 46/47, 507–516.

Gurley, K., Kijewski, T., and Kareem, A. (2001). ''Higher order correlation detection in nonlinear aerodynamic systems using wavelet transforms.'' *Proc. Int. Conf. on Structural Safety and Reliability*, Newport Beach, Calif.

Haan, F. L., Jr., Kareem, A., and Szewczyk, A. A. (1998). ''Effects of turbulence on the pressure distribution around a rectangular prism.'' *J. Wind. Eng. Ind. Aerodyn.*, 77/78, 381–392.

Kareem, A. (1982). ''Acrosswind response of buildings.'' *J. Struct. Eng.*, 108(4), 869–887.

Kareem, A. (1985). ''Lateral-torsional motion of tall buildings.'' *J. Struct. Eng.*, 111(11), 2479–2496.

Kareem, A. (1988). ''Measurements and analysis of pressure fluctuations on prismatic structures in turbulent boundary layer flows.'' *J. Wind. Eng. Ind. Aerodyn.*, 137, 229–235.

Kareem, A. (1990). ''Measurements of pressure and force fields on building models in simulated atmospheric flows.'' *J. Wind. Eng. Ind. Aerodyn.*, 36, 589–599.

Kareem, A. (1997). ''Correlation structure of random pressure fields.'' *J. Wind. Eng. Ind. Aerodyn.*, 69–71, 507–516.

Kareem, A., and Cermak, J. E. (1984). ''Pressure fluctuations on a square building model in boundary-layer flows.'' *J. Wind. Eng. Ind. Aerodyn.*, 16, 17–41.

Kareem, A., and Cheng, C. M. (1984). ''Acrosswind response of towers and stacks of circular cross-section.'' *Rep. No. UHCE 84-5*, Dept. of Civil Engineering, Univ. of Houston, Houston.

Kareem, A., and Zhou, Y. (2002). ''Gust loading factor—Past, present, and future.'' *Proc., Engineering Symp. to Honor Alan G. Davenport for his 40 Years of Contributions*, Univ. of Western Ontario, London, Ont.; also in *J. Wind Eng. Ind. Aerodyn.*, in press.

Kijewski, T., Hann, F., and Kareem, A. (2001). ''Wind-induced vibrations.'' *Encyclopedia of vibration*, S. G., Braun, D. J., Ewins, and S. S., Rao, eds., Academic, New York, 1578–1587.

Kijewski, T., and Kareem, A. (1998). ''Dynamic wind effects: A comparative study of provisions in codes and standards with wind tunnel data.'' *Wind Struct.*, 1(1), 77–109.

Marukawa, H., Ohkuma, T., and Momomura, Y. (1992). ''Acrosswind and torsional acceleration of prismatic high rise buildings.'' *J. Wind. Eng. Ind. Aerodyn.*, 41–44, 1139–1150.

National Research Council of Canada (NRCC). (1996). *User's guide-NBCC1995 structural commentaries (part 4)*, Quibec.

Simiu, E., and Scanlan, R. H. (1996). *Wind effects on structures*, 3rd Ed., Wiley, New York.

Tschanz, T., and Davenport, A. G. (1983). ''The base balance technique for the determination of dynamic wind loads.'' *J. Wind. Eng. Ind. Aerodyn.*, 13, 429–439.

Vickery, P. J., et al. (1985). ''The effect of modal shape on wind-induced response of tall buildings.'' *Proc., 5th U.S. Nat. Conf. on Wind Engineering*, Lubbock, Tex.

Zhou, Y., and Kareem, A. (2001). ''Gust loading factor: New Model.'' *J. Struct. Eng.*, 127(2), 168–175.

Zhou, Y., Kareem, A., and Gu, M. (1999). ''Gust loading factors for design applications.'' *Proc., 10th Int. Conf. on Wind Engineering*, Copenhagen, Denmark, 169–176.

Zhou, Y., Kareem, A., and Gu, M. (2002). ''Mode shape corrections for wind load effects.'' *J. Eng. Mech.*, 128(1), 15–23.